

Recombination dynamics of photodissociated I_2^- in size selected Ar and CO_2 clusters

Vasil Vorsa, Sreela Nandi, Paul J. Campagnola,^{a)} Mats Larsson,^{b)} and W. C. Lineberger
Department of Chemistry and Biochemistry and JILA, University of Colorado and National Institute of Standards and Technology, Boulder, Colorado 80309-0440

(Received 22 August 1996; accepted 15 October 1996)

We report time-resolved photodissociation and geminate recombination dynamics of I_2^- in size-selected $I_2^-Ar_n$ and $I_2^-(CO_2)_n$ cluster ions by using ultrafast pump-probe techniques at 790 nm in conjunction with a tandem time-of-flight mass spectrometer. The absorption recovery, which reflects the time scale for photodissociation followed by recombination and vibrational relaxation of I_2^- inside the cluster, shows a strong dependence on the composition of the surrounding cluster solvent. The absorption recovery time for $I_2^-(CO_2)_{16}$ is ~ 1 ps, whereas for $I_2^-Ar_{20}$ it is ~ 130 ps. This difference is discussed in terms of electrostatic and hard sphere interactions. We also observe the time dependence of the destruction of the Ar solvent cage for $I_2^-Ar_{16}$. Finally, absorption recovery data for $I_2^-(CO_2)_n$ cluster ions taken with 790 nm pump-probe wavelengths are compared with the greater energy release 720 nm data. © 1997 American Institute of Physics.

[S0021-9606(97)01304-4]

I. INTRODUCTION

The concept of solvent-induced recombination of a photodissociated chemical bond was first introduced by Franck, Wood, and Rabinowitch 60 years ago and was termed the ‘‘cage’’ effect.^{1–3} Numerous studies have followed this original work, providing much insight into this chemical process. Many have focused on the geminate recombination yield of dihalogens following photoexcitation in high pressure gases,^{4–9} matrices,^{10–15} and liquids.^{16–19} More recently, picosecond and femtosecond time-resolved studies have been reported on the caging of these dihalogens in liquids,^{20–33} matrices,^{34,35} and high pressure gases^{36,37} as well. Harris and co-workers have measured the rates of each step of the caging process (dissociation, geminate recombination, and vibrational relaxation) of I_2 in various solutions via absorption recovery experiments and have concluded that vibrational relaxation, which is on the order of hundreds of picoseconds, is the rate-limiting process²⁴ in accord with earlier predictions by Nesbitt and Hynes.³⁸ Apkarian and co-workers have carried out time-resolved femtosecond studies exhibiting coherent nuclear motion of I_2 in Ar matrices³⁴ and Kr matrices³⁵ Zewail and co-workers have examined the femtosecond dynamics of I_2 in Ar clusters for the approximate size range of $n=8–40$ and have also reported coherent motion of the I_2 chromophore.^{39,40} In addition, Barbara and co-workers have studied the recombination dynamics of I_2^- in ethanol and other polar solvents.^{41–43} Except for matrix studies, the microscopic behavior of these reactions is often masked by the inherent averaging over many local solvent configurations.

The use of ionic clusters can often simplify this averaging

by mass selection⁴⁴ that enables the effects of solvation to be studied systematically by controlling the number and composition of solvent molecules around the reactant. Although this method can be employed in the study of neutral clusters via post-ionization, clusters often fragment following ionization, complicating the analysis. In addition to precise control of solvent size, ionic clusters are more strongly bound than their neutral counterparts, with the result that the jet cooled ions generally form few isomers, which further contributes to the reduction of averaging. This was observed in our previous studies^{45,46} of I_2^- in CO_2 , where coherent nuclear motion was observed.

Our group has emphasized the recombination of dihalogens in various size-selected cluster ions following photodissociation.^{45–53} Previously, we have reported the time-dependent cage effect in $I_2^-(CO_2)_n$ cluster ions as a function of cluster size following 720 nm excitation.^{45,46,49–52} At this wavelength, up to 0.5 eV kinetic energy release in the I^- and I fragments is possible. Geminate recombination rates were found to be relatively independent of initial cluster size for $n=8–12$ (slow) and for $n=16–22$ (fast) with the rate extremely dependent on cluster size in the size range of $n=12–15$.⁴⁵ Absorption recovery times for $I_2^-(CO_2)_n$ were ~ 30 ps for the smaller precursor size range and ~ 10 ps for the larger range. Both Monte Carlo simulations^{54,55} and experiment⁵¹ indicate that the first CO_2 solvent shell around I_2^- is composed of ~ 16 CO_2 molecules. The simulations also indicate that for the smaller clusters ($n < 5$) the CO_2 molecules bind to the waist of I_2^- and for intermediate size clusters, up to half a solvent shell ($n=8$), the CO_2 molecules preferentially pack around one end of I_2^- .^{54,55} In larger clusters ($n > 8$) the CO_2 molecules begin to enclose the other end of the I_2^- chromophore. It thus might be expected that the recombination rates for I_2^- are independent of cluster size in the smaller and larger clusters, but change rapidly in the size

^{a)}Present address: University of Connecticut Health Center, Center for Biomedical Imaging Technology, CBIT-MC1507, Farmington, CT 06030.

^{b)}Present address: Department of Physics, Royal Institute of Technology, S-100 44 Stockholm, Sweden.

range corresponding to completing the second half of the first solvent shell.

Studies of photodissociated I_2^- in liquids have indicated that recombination rates depend strongly on solvent composition. The absorption recovery time for I_2^- in carbon tetrachloride is ~ 100 ps,²⁴ and increases to nanoseconds in liquid xenon.²⁶ These liquid phase observations raise interesting questions concerning the geminate recombination rates for I_2^- in clusters of different composition. In this work we investigate the time-dependent geminate recombination of $I_2^-Ar_{20}$ following photodissociation at 790 nm and compare these data with corresponding $I_2^-(CO_2)_{16}$ data. Both cluster sizes correspond to approximately one solvent shell around I_2^- . While Ar and CO_2 have similar mass, their electrostatic forces differ considerably. As Ar has no permanent dipole or quadrupole moment while CO_2 has a relatively large quadrupole moment, this experiment enables us to examine the importance of long-range electrostatic forces versus short-range (hard sphere) forces in the geminate cage recombination dynamics of I_2^- . While the above experiment provides information regarding the dynamics of the solute I_2^- , it does not provide detailed insight into the response of the solvent. To understand better the solvent response, we examine the time-dependent breakup of the solvent cage in $I_2^-Ar_{16}$ after 790 nm photoexcitation. Finally, we compare the time-dependent absorption recovery of $I_2^-(CO_2)_n$ clusters at 790 nm with the larger kinetic energy release 720 nm data to gain more insight into this process.

II. EXPERIMENTAL APPARATUS

Time-resolved photofragmentation experiments were carried out by incorporating a tandem time-of-flight (TOF) mass spectrometer in conjunction with a regeneratively amplified Ti:sapphire laser system.

A. Cluster ion source and tandem time-of-flight mass spectrometer

A detailed description of this instrument has appeared elsewhere,^{45,51} so only a brief summary is given here. $I_2^-Ar_n$ and $I_2^-(CO_2)_n$ cluster ions are prepared by expanding 2–3 atm of Ar or CO_2 seeded with $\sim 0.05\%$ iodine vapor through a pulsed valve (General Valve Series 9) with an 800 μm nozzle diameter. This expansion is crossed by a continuous 1 keV electron beam several millimeters below the valve orifice. Attachment of low-energy secondary electrons to I_2^- in the gas expansion produces I_2^- , from which clusters grow via ion–molecule interactions as they drift. The ions drift for ~ 15 cm before entering the first stage of a Wiley–McLaren TOF mass spectrometer.⁵⁶ Negative ions are extracted from this region with a pulsed 1 kV electric field. Upon exiting this region the ions enter a 5 cm acceleration region where they acquire an additional 2.5 keV energy. The $I_2^-Ar_n$ and $I_2^-(CO_2)_n$ cluster ions range up to $n \approx 30$. Intensity anomalies are consistently observed in the $I_2^-Ar_n$ mass spectrum⁴⁷ at $n = 13, 20,$ and 25 . An intensity anomaly is also observed in the $I_2^-(CO_2)_n$ mass spectrum at $n = 16$, consistent with the predicted⁵¹ closure of the first solvent shell.

At the spatial focus of the primary TOF mass spectrometer (located 1.8 m downstream from the extraction region) the cluster ions intersect a pulsed laser beam. A pulsed mass gate located just before this focus transmits only the precursor ion of interest, thus greatly reducing background ion noise on the detectors. Adjustment of the timing between the high voltage extraction pulse and laser pulse establishes mass-selective photoexcitation. Photofragments resulting from the absorption of a photon drift for an additional 5 cm in a field-free region before entering a reflectron TOF mass analyzer.⁵⁷ The reflectron, tilted at a small angle (4°), reverses the trajectory of the ions, separating the precursor and fragment ions according to their mass. Adjustment of the reflectron electric field allows either the precursor ion or the ionic photofragments to be refocused at the off-axis detector with a mass resolution of ~ 700 for parent ions and ~ 300 for fragment ions. The detector assembly consists of a series of acceleration plates followed by a two-plate microchannel plate detector. The acceleration plates increase the kinetic energy of the ions an additional 3 keV to enhance detection efficiency. The detector can be operated in two modes: (1) An analog mode to acquire parent ion mass spectra and one-photon photofragment mass spectra, or (2) a particle counting mode, used to measure two-photon photofragments for time-resolved experiments. When the instrument is set to measure two-photon signal, the electric field in the reflectron is insufficient to reverse the trajectory of the unreacted precursor ions. These precursor ions exit the rear of the reflection and strike the in-line channeltron detector mounted directly behind the reflectron. When operated in this mode, the analog signal from this detector thus provides a measurement of the initial ion intensity and is used to normalize the two-photon photofragment signal to the initial ion intensity.

B. Laser system

The femtosecond laser employed for these time-resolved experiments is a commercial regeneratively amplified Ti:sapphire laser system. A Ti:sapphire oscillator (Coherent Mira Basic) is pumped with 6 W (all lines) from an Ar^+ laser (Coherent Innova 90), thus generating 6 nJ, 110 fs pulses at 790 nm at a repetition rate of 76 MHz. The TEM_{00} output of the Mira laser is first stretched to ~ 150 ps with a Quantronix 4800 Series Stretcher & Compressor before entering a Ti:sapphire regenerative amplifier (Quantronix 4800 RGA). The amplifier, pumped by a frequency doubled Nd:YLF laser (Quantronix) at 10 mJ per pulse at 527 nm, amplifies the stretched pulses to ~ 2 mJ at 400 Hz. The pulses are then compressed to ~ 140 fs with a ~ 1.0 mJ/pulse energy. Although the amplified laser pulse widths are ~ 140 fs, the manner in which we focus and cross our laser beams at the laser interaction region degraded the effective resolution to ~ 1 ps.

Pump and probe laser pulses are generated by splitting this output into two identical pulses using a 50/50 beam splitter. The two beams travel different optical paths to the laser interaction region of the mass spectrometer where they

cross at an angle of $\sim 5^\circ$. Both laser beams were focused to a spot size of $\sim 4\text{--}5$ mm diameter at this region. The temporal delay between the pump and probe laser beams is accomplished by the use of a computer controlled optical delay line with a resolution of <10 fs. The electric field vectors for both the pump and probe beams were parallel to the ion velocity vector of the ion beam for all experiments reported here. The probe pulse should normally be polarized at the magic angle with respect to the pump pulse in order to eliminate a spurious time dependence due to the decay of rotational anisotropy. For the Ar cluster data, the recovery times are sufficiently long and the Ar solvent evaporation is so extensive that the difference is unimportant. For the larger CO_2 cluster data, the exact form of the early time absorption does depend on the probe polarization,⁴⁵ but for the qualitative conclusions reported here the difference is unimportant.

The repetition rate of the pulsed ion beam is limited to 80 Hz as a result of ion source pumping speed limitations. Synchronization of the ion signal to the laser is accomplished by sending a 400 Hz trigger pulse from the Pockels cell driver to a counter that provides an output pulse on every fifth trigger pulse. Precise temporal overlap of the ions with the laser is accomplished through the use of a delay generator (Stanford DG 535) to trigger the pulsed valve and provide an ion extraction pulse.⁴⁴

C. Data collection

Detecting negative ions on the microchannel plate detector can involve voltages up to 7.5 kV on the anode of this detector, requiring capacitive coupling of the ion signal to the (grounded) signal processing electronics. The capacitively coupled ion pulse signals are preamplified (Ortec 9301) by a factor of 10 and split into two parts. While one part is directed to an oscilloscope for continuous monitoring, the other is sent to either a transient digitizer/signal averager (Transiac 2001S/4100) for recording parent and photofragment mass spectra or to particle counting electronics. For particle counting experiments (time-resolved experiments), a 300 MHz discriminator (Phillips Scientific 6904) is inserted after the preamplification step to reject electrical noise associated with detector electronics, while passing real signal counts. This output is then sent to either a Stanford Research Systems counter (SR620) or a CAMAC controlled DSP quad scaler (DSP QS-450) with the capability of measuring counts on four separate channels simultaneously. Signals measured by the SR620 counter were sent to the computer through a GPIB interface. All other signals were sent to the computer through the CAMAC controller (DSP 6001).

The $I_2^-Ar_n$ ion intensity was approximately an order of magnitude smaller than the $I_2^-(CO_2)_n$ precursor ion signal, thus requiring longer averaging for the absorption recovery measurements. Each data point in the absorption recovery curves for $I_2^-Ar_n$ clusters consisted of 5000–10 000 laser pulses. Background measurements consisting of 5000–10 000 laser pulses followed every ninth cross section measurement. The 790 nm $I_2^-(CO_2)_n$ data were acquired with

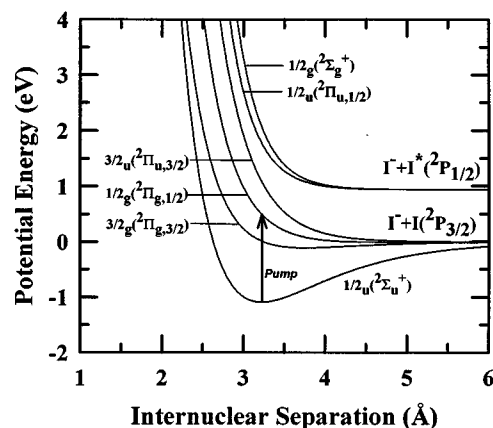


FIG. 1. Semiempirical gas phase potential energy curves for I_2^- (Refs. 58 and 59). Each electronic state is identified with the Hund's case (c) symmetry label. The arrow labeled *pump* indicates the transition used to photodissociate I_2^- .

2500–5000 laser pulses, with correspondingly fewer background measurements.

III. DESCRIPTION OF PUMP-PROBE EXPERIMENT

Semi-empirical gas phase potential energy curves for I_2^- are shown in Fig. 1. The ground state is characterized by a bond order of $\frac{1}{2}$, $\omega_e \sim 115$ cm^{-1} , and $D_0 \sim 1.1$ eV.^{58,59} All remaining electronic states in the bare ion are repulsive. The arrow in Fig. 1 indicates the $\frac{1}{2}g(2\Pi_{g,1/2}) \leftarrow \frac{1}{2}u(2\Sigma_u^+)$ transition used to photodissociate the I_2^- , producing $I^- + I$ with a kinetic energy release of ~ 0.5 eV. Depending on the size of the cluster, the separating I atoms will either escape (uncaged) or be forced back together (caged) to reform the I_2^- bond. Measuring the time scale of this cycle (dissociation, recombination, and vibrational relaxation) is the major goal of these pump-probe experiments.

Since a qualitative understanding of the experiment is essential for data interpretation, a brief summary is given here. A detailed description of the data acquisition algorithm is available.⁴⁵ A size-selected $I_2^-X_n$ cluster ion absorbs a 790 nm photon from an ultrafast pump pulse, dissociating the I_2^- chromophore. Immediately following photodissociation of I_2^- , the cluster ion is transparent to 790 nm radiation. Only when the I_2^- has reached a region of the potential energy surface with an appreciable absorption cross section at 790 nm can the cluster absorb a second photon from a probe pulse of the same color. One such region corresponds to vibrationally relaxed I_2^- . Monitoring the absorption recovery from this region measures the time for caging and vibrational relaxation (complete absorption recovery). Absorption of *one* photon results in a narrow photofragment distribution corresponding to the evaporation an average number k_{evap} of solvent monomers. This class of fragments is referred to as *one-photon* products. Absorption of a second photon results in the evaporation of additional; these fragments are referred to as *two-photon* products. All three groups—precursor, one-photon products, and sequential two-photon products—are readily separated by the secondary mass analyzer (reflec-

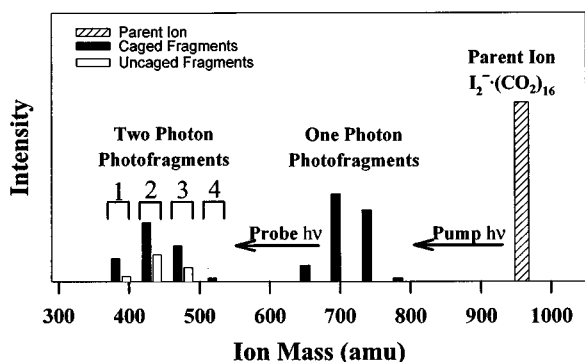


FIG. 2. Histogram of the photofragment ion distribution for $I_2^-(CO_2)_{16}$ after absorbing one and two 790 nm photons. The absorption of one-photon results in a 100% caged photofragment distribution, while absorption of two-photons results in caged and uncaged fragments. The cross-hatched bar represents the parent ion, filled bars represent caged photofragment ions, and open bars represent uncaged photofragment ions.

tron). While the same general considerations apply to both Ar and CO_2 cluster ions, an example specific to $I_2^-(CO_2)_{16}$ is shown in Fig. 2. The parent $I_2^-(CO_2)_{16}$ absorbs one 790 nm photon from the pump pulse and fragments into $I_2^-(CO_2)_{8,9,10}$. These photoproducts can then absorb a second photon from a probe pulse, to produce lighter caged, $I_2^-(CO_2)_{2,3,4}$, and uncaged, $I_2^-(CO_2)_{5,6,7}$, ionic fragments. The absorption recovery is thus mapped out by measuring the total number of sequential two-photon products produced as a function of the delay between pump and probe laser pulses.

For the $I_2^-Ar_{16}$ time-dependent solvent cage breakup experiment, four two-photon product channels were monitored separately. This was accomplished by the use of a gated quad scaler, as indicated in Fig. 2 with the gates numbered 1 through 4. The positions and widths of these gates can be adjusted independently, allowing observation of the signal from any photoproduct channel.

IV. RESULTS AND DISCUSSION

The primary goal of this work is to study the time-dependent photodissociation and recombination dynamics of I_2^- in size-selected Ar and CO_2 clusters. In Sec. A the absorption recovery of $I_2^-Ar_{20}$ is presented and compared with that of $I_2^-(CO_2)_{16}$. The difference in the observed absorption recovery rates is discussed in terms of long-range electrostatic and short-range (hard-sphere) interactions. In Sec. B, we present data exhibiting the time-dependent breakup of the solvent cage for $I_2^-Ar_{16}$ after the absorption of one 790 nm photon. A simple model is developed to provide a time-dependent picture of the breakup of the Ar cluster around I_2^- . In Sec. C, we present time-dependent absorption recovery data for $I_2^-(CO_2)_{6,9,13,16}$ cluster ions at 790 nm and compare these data with the corresponding 720 nm data, where the kinetic energy release is ~ 150 meV greater.

A. I_2^- absorption recovery in Ar and CO_2 clusters

Absorption recovery experiments were carried out on $I_2^-Ar_{20}$ and $I_2^-(CO_2)_{16}$ to investigate the role of long-range

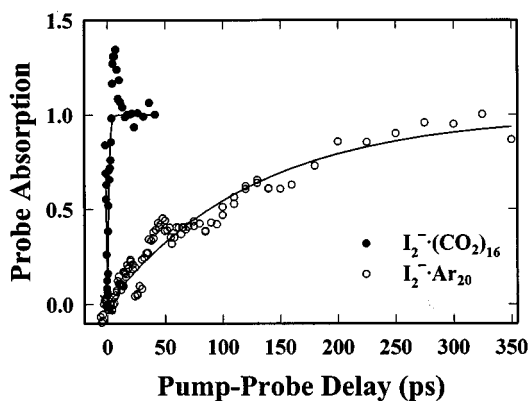


FIG. 3. Absorption recovery data for $I_2^-Ar_{20}$ (open circles) and $I_2^-(CO_2)_{16}$ (filled circles) obtained with parallel pump-probe polarization at 790 nm. The smoothing algorithm used to remove high frequency noise from the $I_2^-Ar_{20}$ data is described in the text. Also shown are exponential fits of the form $1 - e^{-t/\tau}$. The time constants obtained from this fit are 127 ± 4 ps and 1.3 ± 0.1 ps, respectively.

electrostatic interactions versus hard-sphere interactions on the cage recombination dynamics of I_2^- in a cluster. These particular cluster sizes were chosen so that approximately one complete solvent shell surrounded the I_2^- chromophore. For $I_2^-(CO_2)_n$ this occurs at $n \approx 16$,⁵¹ and for $I_2^-Ar_n$ this occurs for 20–25 Ar atoms.⁴⁷ Figure 3 depicts the absorption recovery signal for $I_2^-Ar_{20}$ and $I_2^-(CO_2)_{16}$ taken with 790 nm pump and probe wavelength. This signal is the sum of all ion counts arising from absorption of both one pump proton and one probe photon, normalized to the parent ion intensity and the energy of the pump and probe photon pulses.⁴⁵ As the pump and probe wavelengths are the same, the signal here (and in the subsequent figures) should be symmetric about $t=0$. In fact, this symmetry, coupled with the rapid rise in the $I_2^-(CO_2)_{16}$ signal, are used to determine accurately zero time delay.⁴⁵ The $I_2^-Ar_{20}$ absorption recovery data contained high frequency shot noise normally associated with low signal level counting experiments. The data shown here were smoothed using a five-point running average (except for the three points nearest zero delay, where such averaging would extend to negative time) to remove high frequency noise from the absorption recovery signal. Immediately evident is the hundred-fold decrease in the absorption recovery rate of $I_2^-Ar_{20}$ compared with that of $I_2^-(CO_2)_{16}$. Also shown in the figure are simple exponential fits to the data of the form $1 - e^{-t/\tau}$. The time constants are 127 ± 4 ps and 1.3 ± 0.1 ps, respectively. The “overshoot” in the $I_2^-(CO_2)_{16}$ curve will be discussed in Sec. C.

The striking difference in recovery times between the two solvents might arise from several possibilities. One involves the rate at which the caged I_2^- undergoes recombination into the ground electronic state. It has been shown in simulations⁵⁴ that in the presence of a solvent electric field, the I_2^- potential energy surfaces shift significantly, especially at larger internuclear separations. Since the greatest probability of recombination onto the ground electronic state occurs at longer bond lengths where the potential surfaces become

nearly degenerate, a shift in the potential energies in this region is expected to have a significant effect on the absorption recovery rate. Since CO₂ has a large quadrupole moment (-4.3×10^{-26} esu cm²)⁶⁰ with an approximate charge distribution of $-\frac{1}{2}$ on each oxygen and +1 on the carbon atom, it is possible that the rate of I₂⁻ recombination is significantly influenced by strong perturbations of the I₂⁻ potentials with the electric fields generated by the CO₂ solvent. Conversely, as Ar does not have a dipole or quadrupole moment, we expect it does not alter the I₂⁻ potentials as significantly. However, without further information it is difficult to speculate as to which direction this rate will shift relative to the CO₂ solvent. Several other processes in the cage recombination dynamics, however, also contribute to the overall absorption recovery rate.

Another potentially important rate-limiting process is vibrational relaxation of the I₂⁻ in the ground electronic state. The rate of this process depends on the efficiency of the energy transfer from the solute I₂⁻ to the solvent Ar or CO₂ bath. Simulations suggest⁵⁴ that vibrational relaxation of I₂⁻ proceeds rapidly inside CO₂ clusters, losing ~ 1 eV in several picoseconds. Since Ar and CO₂ have approximately the same mass, 40 and 44 amu, respectively, the kinematic component of the vibrational to translational energy transfer rate is expected to be similar for the two solvents. However, since Ar creates weaker solvent electric fields relative to CO₂, the electrostatic vibrational to solvent coupling will be weaker. This can lead to slower vibrational relaxation of I₂⁻ inside an Ar cluster. However, simulations⁵⁴ indicate that this effect is not very large, suggesting that other mechanisms may be more important.

One such mechanism involves the vibrational energy transfer from the I₂⁻ chromophore to the internal vibrational and rotational degrees of freedom of the solvent. Although efficient I₂⁻ vibrational to CO₂ internal vibrational mode energy transfer is unlikely in I₂⁻(CO₂)_n clusters, because the lowest vibrational frequency in CO₂ is 667 cm⁻¹ (115 cm⁻¹ for I₂⁻), vibrational to rotational and/or librational energy transfer is likely quite efficient. Several of the solid CO₂ lattice frequencies are very close to the 115 cm⁻¹ harmonic vibrational frequency of I₂⁻.^{58,59} The A_u, E_u, T_u, T_u(Q₁) (translational), and the T_g(Q₁) (librational) lattice vibrations have frequencies of 109.4, 116.9, 117.2, and 136 cm⁻¹, respectively. On the other hand, the largest frequency that solid Ar can support, the Debye frequency, is ~ 64 cm⁻¹.⁶¹ These additional degrees of freedom, as well as possibly more efficient energy transfer, likely lead to the more rapid vibrational relaxation of I₂⁻ in CO₂ clusters.

A third possible rate-limiting process may involve the strength of the cluster cage itself. As previously mentioned, the large quadrupole moment of CO₂ leads to strong coupling between the excess negative charge on the iodine chromophore and CO₂. The large quadrupole moment also leads to stronger CO₂-CO₂ binding compared to Ar. The net result is a cohesive CO₂ solvent cage that forms around the I₂⁻. Because Ar lacks large electrostatic moments, its binding energy to the cluster is about a factor of 3 smaller,⁴⁷ and, in addition, the weaker Ar-Ar interactions lead to a weaker

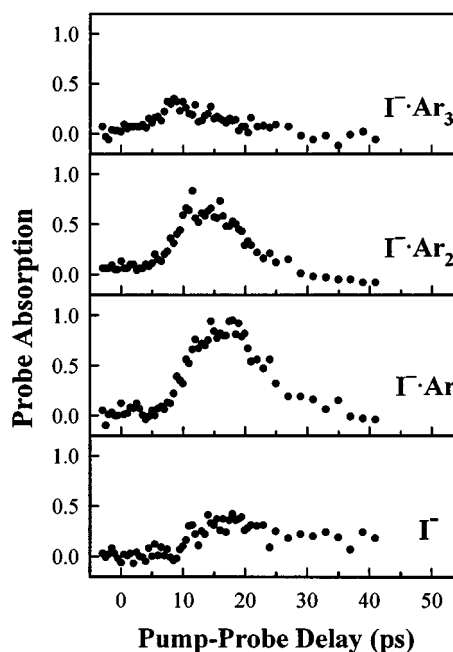


FIG. 4. Absorption recovery data for I₂⁻Ar₁₆ obtained with parallel pump-probe polarization at 790 nm. Each curve corresponds to the absorption recovery as measured by the indicated photoproduct.

solvent cage network around I₂⁻, compared to that of CO₂. Hence, the dissociating I atoms may separate to longer internuclear distances, thus allowing the possibility for an Ar atom to move between the I and I⁻ atoms and impede the recombination process. The 790 nm absorption recovery rate for I₂⁻(CO₂)₁₆ is similar to the rates observed for I₂⁻ in ethanol and other polar solvents in this wavelength region,⁴¹⁻⁴³ where it was determined that vibrational relaxation in the lower 30% of the ground state well is the rate-limiting process in the overall absorption recovery.

B. Time-resolved breakup of I₂⁻Ar₁₆

In this section we examine the solvent cage breakup of the I₂⁻Ar₁₆ cluster ion after absorption of a single 790 nm (1.57 eV) photon. Photofragmentation experiments indicate that the only caged photoproduct resulting from single photon excitation of I₂⁻Ar₁₆ is I₂⁻. This result indicates that the only two-photon product at long delay time is I⁻ and suggests that at any delay time it is also I⁻. When the two-photon products were studied with ultrafast pump-probe pulses, however, we found a new class of products at intermediate delay times, not seen in any of our earlier photofragmentation studies.^{45,47,48,51,53,62} These products are *transient* two-photon I⁻Ar_m products. Since these photofragments arise from clusters still undergoing evaporation, the transient nature of the I⁻Ar_m signal allows us to construct a time-dependent picture of the breakup of the I₂⁻Ar₁₆ cluster ion.

Figure 4 shows the absorption recovery signal of I₂⁻Ar₁₆ as monitored by the appearance of I⁻, I⁻Ar, I⁻Ar₂, and I⁻Ar₃ as a function of pump-probe delay. All channels, ex-

cept I⁻, are transient, beginning with zero signal, peaking at some finite pump–probe delay time, and then decaying to zero. The I⁻ channel has a much slower signal decay rate and does not decay to zero at long pump–probe delays. A more sophisticated model incorporating Ar atom evaporation is required to interpret these data.

We begin by examining the two-photon I⁻ signal. From previous single photon excitation experiments⁴⁷ we know that a caged photoproduct arising from a large I₂⁻Ar_{*n*} cluster after absorbing a 790 nm photon evaporates ~21 Ar atoms. This indicates that, on average, ~73 meV goes into the evaporation (binding and kinetic energy) of each Ar atom from the cluster. Therefore, following absorption of a 790 nm photon, the I₂⁻Ar₁₆ cluster undergoes complete evaporation. Since this number is five Ar atoms fewer than what is needed to remove all of the initial photon energy, the I₂⁻ photoproduct must have ~0.4 eV vibrational excitation.

To obtain a time-dependent picture of the solvent cage breakup, the size of the cluster at the time of absorption of the second photon must be determined. In the case of large cluster ions, we expect the early evaporation dynamics to be largely governed by short-range interactions. In particular, Ar atoms which are collinear with the I₂⁻ bond are ejected rapidly from the cluster with a substantial amount of kinetic energy, resulting in a cluster with no Ar atoms capping I₂⁻. Absorption of a second photon leads to escape of I and I⁻ with relatively little interaction with the remaining Ar atoms. This case is similar to the absorption of a single photon in smaller clusters (*n* < 10), where the Ar atoms are likely bound around the waist of I₂⁻. The photoproduct distribution from these clusters should also be relatively independent of the kinetic energy release since most of this energy is expected to be imparted into the dissociating I and I⁻ fragments. Therefore, the final fragment distributions from both cases likely originate from similar cluster sizes. In the one case, it is time *independent*, arising from the precursor cluster ion and in the other, it is time *dependent* arising from a cluster undergoing evaporation.

Figure 5 displays the average number of Ar atoms remaining on the I⁻-based photoproducts 10 μs after absorbing one 790 nm photon as a function of cluster size. The width of the photoproduct distribution is ~3 Ar atoms for all cluster sizes. Assuming that the one-photon product distribution does not depend strongly on the amount of kinetic energy release of the dissociating I atoms, as discussed above, we can estimate the size of the evaporating cluster at the time it absorbed the second photon. Using these data and the data in Fig. 4, we can construct a time-dependent picture of the breakup of the Ar solvent cage around the I₂⁻ by relating the peak times of these photoproducts to which cluster size they originated from. For example, the I⁻Ar₃ product peaks ~8 ps after excitation of I₂⁻Ar₁₆, suggesting that in ~8 ps following absorption of the initial photon, the I₂⁻Ar₁₆ cluster ion has evaporated ~6 Ar atoms. Following the same logic for the other products, we find that in ~13 ps the I₂⁻Ar₁₆ cluster ion has evaporated ~8 Ar atoms and in ~17 ps I₂⁻Ar₁₆ cluster ion has evaporated ~10 Ar atoms. This model provides a qualitative time scale for the evaporation of Ar atoms from

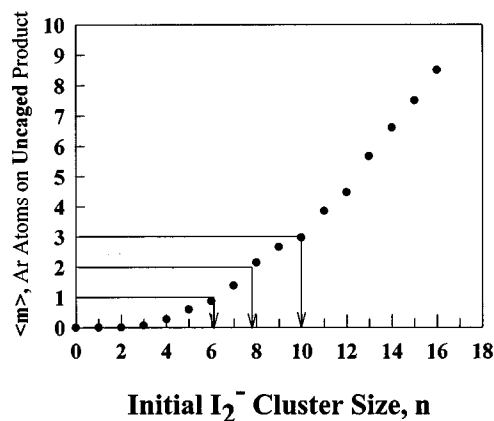
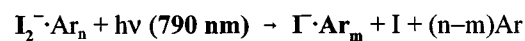


FIG. 5. Average number $\langle m \rangle$ of Ar atoms remaining on the uncaged (I⁻-based) photofragments following absorption of one 790 nm photon as a function of initial cluster size *n*.

the I₂⁻Ar₁₆ cluster ion after absorbing one 790 nm photon. The initial breakup of the solvent cage proceeds very rapidly, losing ~6 Ar atoms in ~8 ps. The remaining 6 Ar atoms take >17 ps to evaporate.

C. Time-dependent caging of I₂⁻(CO₂)_{*n*} cluster ions at 790 nm

Previous 720 nm pump–probe experiments⁴⁵ suggested that for I₂⁻(CO₂)_{*n*} clusters in the range of *n* = 8–12, the photodissociated I₂⁻ chromophore is able to undergo large amplitude motion before recombination, thus allowing the possibility of a CO₂ molecule to enter the space between the dissociating I atoms, producing a transient solvent separated I⁻–I pair. Conversely, as more CO₂ molecules are added to the solvent cage, the I⁻–I motion becomes increasingly restricted, forcing the two I atoms to remain a “contact pair” and producing rapid recombination. Two characteristic absorption recovery time scales were observed in these experiments for two cluster size regimes. Upon 720 nm photoexcitation of clusters in the range of *n* = 8–12, absorption recovery occurs in ~30–40 ps. For cluster sizes *n* = 15–22 the time is ~10 ps. Clusters of intermediate size (*n* = 13 and 14) display a transition between the two absorption recovery time scales.

Absorption recovery measurements for I₂⁻(CO₂)_{*n*} were repeated at 790 nm using the Ti:sapphire laser system. Figure 6 depicts the 790 nm absorption recovery data for I₂⁻(CO₂)_{6,9,13,16}. The kinetic energy release is ~470 meV compared to ~620 meV with 720 nm. The data show a gross cluster size dependence consistent with the earlier 720 nm data.⁴⁵ Excitation at 790 nm results in more rapid absorption recovery at any given cluster size. Included in the figure are simple exponential fits (solid lines) of the form $1 - e^{-t/\tau}$, appropriate for a simple two level kinetic model. The absorption recoveries of *n* = 6, 9, 13 are fit remarkably well by this simple exponential form, and even though the *n* = 16 data has an overshoot, the fit provides a qualitative value for τ that

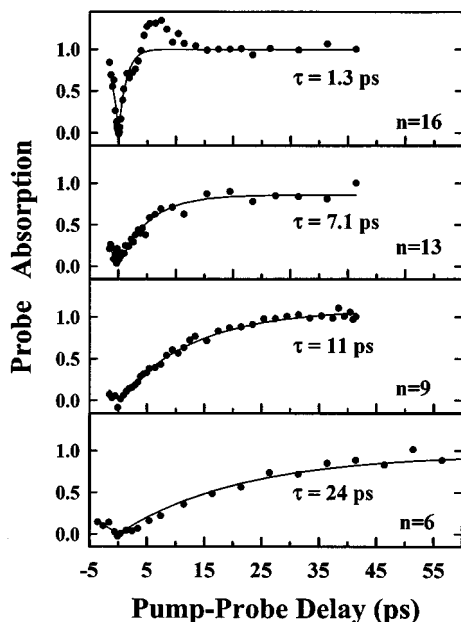


FIG. 6. $I_2^-(CO_2)_n$ ($n=6, 9, 13,$ and 16) absorption recovery data obtained with 790 nm pump and probe pulses with parallel polarization. Also shown are exponential fits of the form $1 - e^{-t/\tau}$. The time constants are noted in the figure.

can be compared to other cluster sizes. Table I lists these time constants as a function of cluster size for both 790 nm and 720 nm. Although none of the 720 nm absorption recoveries⁴⁵ exhibit simple exponential behavior, these times still provide a useful qualitative comparison.

We attribute the difference in the 720 nm absorption recovery rates between the two cluster size regimes ($n=8-12$ and $n=15-22$) to the completion of the first solvent shell, which occurs approximately at $n=16$. Figure 7 depicts the 790 nm time-dependent evaporation process for that subset of photodissociated cluster ions which successfully recombine. Shown in this figure are the initial cluster size, the final cluster size following photoexcitation and recombination, and the respective absorption recovery time. A comparison of the number of CO_2 molecules remaining following the

TABLE I. Absorption recovery time constant τ as a function of $I_2^-(CO_2)_n$ precursor ion size for 720 nm and 790 nm. τ was extracted from a $1 - e^{-t/\tau}$ fit to the data.

| n | τ (ps) | |
|-----|----------------|----------------|
| | 720 nm | 790 nm |
| 6 | ... | 23.7 ± 1.4 |
| 8 | 22.7 ± 1.0 | ... |
| 9 | 21.4 ± 0.7 | 10.9 ± 0.4 |
| 12 | 21.4 ± 1.1 | ... |
| 13 | 16.1 ± 0.9 | 7.1 ± 0.5 |
| 14 | 11.2 ± 0.3 | ... |
| 15 | 8.9 ± 0.5 | ... |
| 16 | 6.9 ± 0.2 | 1.3 ± 0.2 |
| 17 | 7.6 ± 0.4 | ... |
| 22 | 5.2 ± 0.3 | ... |

| | Absorption Recovery Time Constant | | | |
|--------------------|-----------------------------------|--------|-------|-------|
| | 1.3 ps | 7.1 ps | 11 ps | 24 ps |
| Precursor | | | | |
| $I_2^-(CO_2)_{16}$ | ↓ | | | |
| $I_2^-(CO_2)_{15}$ | | | | |
| $I_2^-(CO_2)_{14}$ | | | | |
| $I_2^-(CO_2)_{13}$ | | ↓ | | |
| $I_2^-(CO_2)_{12}$ | | | | |
| $I_2^-(CO_2)_{11}$ | ↓ | | | |
| $I_2^-(CO_2)_{10}$ | | | | |
| $I_2^-(CO_2)_9$ | | ↓ | | |
| $I_2^-(CO_2)_8$ | | | | |
| $I_2^-(CO_2)_7$ | | ↓ | | |
| $I_2^-(CO_2)_6$ | | | ↓ | |
| $I_2^-(CO_2)_5$ | | | | |
| $I_2^-(CO_2)_4$ | | | ↓ | |
| $I_2^-(CO_2)_3$ | | | | |
| $I_2^-(CO_2)_2$ | | | | |
| $I_2^-CO_2$ | | | | ↓ |
| I_2^- | | | | |

FIG. 7. Schematic diagram depicting the initial and final cluster ion sizes of evaporation following 790 nm photoexcitation and the time scale of evaporation. An approximate time scale of evaporation can be obtained for specific cluster ion size regions by comparing absorption recovery time constants of clusters with common ionic photofragment sizes.

absorption of one 790 nm photon provides insight into the reason the absorption recovery time for $I_2^-(CO_2)_6$ is much slower than for $I_2^-(CO_2)_9$. Since both of these clusters are expected to undergo large amplitude motion due to their incomplete solvent cages, the difference in their absorption recovery rates must arise from differences in the size of the cluster solvent. While $I_2^-(CO_2)_9$ evaporates down to an average cluster size of $I_2^-(CO_2)_3$, the $I_2^-(CO_2)_6$ cluster ion evaporates to I_2^- . The difference in the rate of absorption recovery between these two cluster ions must, therefore, arise from the time required to evaporate the last several CO_2 molecules from the $I_2^-(CO_2)_n$ cluster. A lower limit on the rate of evaporation of the final three CO_2 molecules from $I_2^-(CO_2)_6$ can be obtained by taking the difference in the absorption recovery rates for the two cluster sizes. This difference yields ~ 13 ps as a lower limit for the time required to evaporate the last several CO_2 molecules.

The most striking feature in the 790 nm data, not observed at 720 nm, is the overshoot in the absorption recovery signal for $I_2^-(CO_2)_{16}$ (see Fig. 8). The origin of this feature is not clear, but it is not believed to arise from coherent nuclear motion. The overshoot likely arises from a 790 nm absorption cross section that is greater for excited vibrational states than it is for vibrational levels near the ground state. This is consistent with several observations. First, the absorption recovery signal immediately following the overshoot is constant, suggesting that the overshoot occurs when the I_2^- has relaxed close to the bottom of the ground state potential. Second, a simple model of the temperature dependence of the I_2^- absorption cross section incorporating a thermal

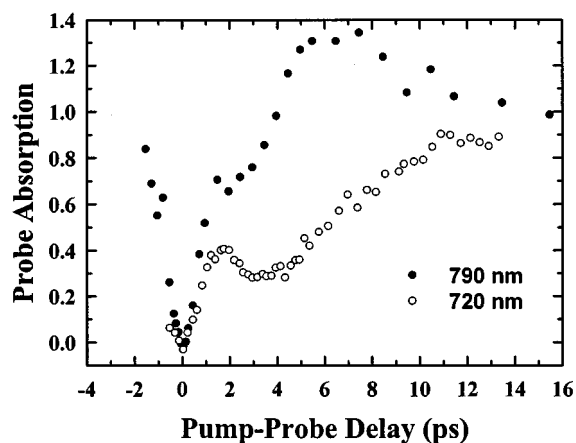


FIG. 8. Expanded view of $I_2^-(CO_2)_{16}$ absorption recovery obtained with 790 nm (filled circles) and 720 nm (open circles) excitation. The laser pulse widths were 150 fs and 280 fs, respectively.

Boltzmann distribution indicates that the overall absorption cross section is very sensitive to the I_2^- vibrational temperature at 790 nm, the red wing of the photodissociation spectrum. Cooling the population from 300 K to 100 K in this model produced a change in the absorption cross section that was qualitatively similar to that observed experimentally. Although not as pronounced, this feature was observed for $n=13$. The overshoot was not observed for the smaller CO_2 cluster ions, which may indicate that the one-photon products of these clusters do not cool as efficiently as the photo-products from the larger clusters ions. This is consistent with the larger binding energies generally observed for the first several solvent atoms or molecules bound to an ionic chromophore.^{63,64} Larger binding energies enable clusters to stay intact at greater temperatures.

Barbara and co-workers^{41,42} observed a similar overshoot in time-resolved absorption recovery measurements of I_2^- in polar solvents at room temperature. In these studies, the pump laser pulse was fixed at 770 nm and the probe wavelength was varied from 580 nm to 950 nm. They found that vibrationally excited states in the bottom 30% of the ground electronic will have an appreciable absorption cross section at longer and shorter wavelengths. In their work, an overshoot was observed for probe wavelengths <600 nm and >820 nm.

The feature at ~ 2 ps in the 720 nm data arises from coherent nuclear motion of the two I atoms in the first excited state of the I_2^- .⁴⁵ Closer inspection of the curves in Fig. 8 shows that this feature is still present in the 790 nm data, but is much less pronounced and appears more as a shelf than a “bump.” This may well be due to the effective time resolution of our experiment compared with the earlier 720 nm experiments. Although the amplified laser pulse widths were on the order of 140 fs, the manner in which we focus and cross our laser beams at the laser interaction region degraded the effective resolution to ~ 1 ps. Observation of this feature at approximately the same time as was observed at 720 nm, however, supports the conclusion of coherent motion taking place on this first excited state. Moreover, it pre-

sents strong evidence that the overshoot at ~ 5 ps does not arise from coherent nuclear motion of I_2^- .

V. CONCLUSIONS

We have carried out pump-probe experiments on size selected $I_2^-Ar_n$ and $I_2^-(CO_2)_n$ cluster ions at 790 nm. Three sets of experiments investigate different aspects of the caging process. First, the absorption recovery signals for $I_2^-Ar_{20}$ and $I_2^-(CO_2)_{16}$ were measured to investigate the role of hard-sphere interactions versus long-range electrostatic interactions on the overall rate of recombination and vibrational relaxation of I_2^- inside a cluster with approximately one solvent shell. A simple exponential fit to the data yielded an absorption recovery time of ~ 130 ps for $I_2^-Ar_{20}$ and ~ 1.3 ps for $I_2^-(CO_2)_{16}$, indicating that long-range electrostatic forces play a significant role in overall cage recombination rate. Time-resolved experiments on the solvent cage breakup of $I_2^-Ar_{16}$ showed that the evaporation process initially proceeds rapidly, evaporating 6 Ar atoms within approximately 8 ps, slowing to approximately several picoseconds per Ar atom. Finally, the 790 nm absorption recovery data for $I_2^-(CO_2)_{6,9,13,16}$ is presented and compared to the data taken at 720 nm. While the gross cluster size dependence is consistent with the earlier 720 nm data, the 790 nm data display a more rapid increase in the absorption recovery. Additionally, we determine a lower limit of ~ 13 ps for the time required to evaporate the last several CO_2 molecules from $I_2^-(CO_2)_n$ cluster ions by comparing the absorption recovery rates of $I_2^-(CO_2)_6$ and $I_2^-(CO_2)_9$.

$I_2^-X_n$ cluster ions have proven to be excellent systems for studying the effects of solvent-induced cage recombination in a precise stepwise fashion. The experiments presented here provide insight into the effects of hard-sphere and long-range electrostatic forces on caging as well as the time-dependent evaporation of the solvent cage. Future work on I_2^- caging in other cluster solvents such as Xe, CS_2 , N_2O , and OCS will shed further light on the interactions which are most important in caging.

ACKNOWLEDGMENTS

We are pleased to acknowledge many stimulating discussions with James Faeder, Dr. Doo Wan Boo, Dr. John Papanikolas, Professor Robert Parson, and Professor Stephen Leone. This research was supported by NSF Grant No. CHE93-18639 and PHY95-12150. M.L. was supported by the JILA Visiting Fellowship program.

¹E. Rabinowitch and W. C. Wood, *Trans. Faraday Soc.* **32**, 1381 (1936).

²E. Rabinowitch and W. C. Wood, *Trans. Faraday Soc.* **32**, 547 (1936).

³J. Franck and E. Rabinowitch, *Trans. Faraday Soc.* **30**, 120 (1934).

⁴H. Hippler, V. Schubert, and J. Troe, *J. Chem. Phys.* **81**, 3931 (1984).

⁵B. Otto, J. Schroeder, and J. Troe, *J. Chem. Phys.* **81**, 202 (1984).

⁶K. Luther, J. Schroeder, J. Troe, and U. Unterberg, *J. Phys. Chem.* **84**, 3072 (1980).

⁷J. Troe, *Ann. Rev. Phys. Chem.* **29**, 223 (1978).

⁸K. Luther and J. Troe, *Chem. Phys. Lett.* **24**, 85 (1974).

⁹H. Hippler, K. Luther, and J. Troe, *Chem. Phys. Lett.* **16**, 174 (1972).

¹⁰J. G. McCaffrey, H. Kunz, and N. Schwentner, *J. Chem. Phys.* **96**, 2825 (1992).

- ¹¹H. Kunz, J. G. McCaffrey, R. Schrieffer, and N. Schwentner, *J. Chem. Phys.* **94**, 1039 (1991).
- ¹²V. E. Bondybey and L. E. Brus, *Adv. Chem. Phys.* **41**, 269 (1980).
- ¹³V. E. Bondybey and C. Fletcher, *J. Chem. Phys.* **64**, 3615 (1976).
- ¹⁴V. E. Bondybey, S. S. Bearder, and C. Fletcher, *J. Chem. Phys.* **64**, 5243 (1976).
- ¹⁵P. B. Beeken, E. A. Hanson, and G. W. Flynn, *J. Chem. Phys.* **78**, 5892 (1983).
- ¹⁶P. S. Dardi and J. S. Dahler, *J. Chem. Phys.* **93**, 242 (1990).
- ¹⁷G. N. R. Tripathi, R. H. Schuler, and R. W. Fessenden, *Chem. Phys. Lett.* **113**, 563 (1985).
- ¹⁸L. F. Meadows and R. M. Noyes, *J. Am. Chem. Soc.* **82**, 1872 (1960).
- ¹⁹D. Booth and R. M. Noyes, *J. Am. Chem. Soc.* **82**, 1868 (1960).
- ²⁰X. Xu, S. Yu, R. Lingle, H. Zhu, and J. B. Hopkins, *J. Chem. Phys.* **95**, 2445 (1991).
- ²¹R. Lingle, X. Xu, S. Yu, H. Zhu, and J. B. Hopkins, *J. Chem. Phys.* **93**, 5667 (1990).
- ²²R. Lingle, S. Xu, S. Yu, Y. J. Chang, and J. B. Hopkins, *J. Chem. Phys.* **92**, 4628 (1990).
- ²³M. E. Paige and C. B. Harris, *Chem. Phys.* **149**, 37 (1990).
- ²⁴A. L. Harris, J. K. Brown, and C. B. Harris, *Annu. Rev. Phys. Chem.* **39**, 341 (1988).
- ²⁵D. E. Smith and C. B. Harris, *J. Chem. Phys.* **87**, 2709 (1987).
- ²⁶M. E. Paige, D. J. Russell, and C. B. Harris, *J. Chem. Phys.* **85**, 3699 (1986).
- ²⁷A. L. Harris, M. Berg, and C. B. Harris, *J. Chem. Phys.* **84**, 788 (1986).
- ²⁸M. Berg, A. L. Harris, and C. B. Harris, *Phys. Rev. Lett.* **54**, 951 (1985).
- ²⁹P. Bado, C. Dupuy, D. Magde, K. R. Wilson, and M. M. Malley, *J. Chem. Phys.* **80**, 5531 (1984).
- ³⁰P. Bado, P. H. Berens, and K. R. Wilson, in *Proc. Soc. Photo-Opt. Instrum. Eng.* **322**, 230 (1982).
- ³¹D. F. Kelley, N. A. Abul-Haj, and D. Jang, *J. Chem. Phys.* **80**, 4105 (1984).
- ³²C. A. Langhoff and W. Nugent, in *Picosecond Phenomena II: Proceedings of the Second International Conference on Picosecond Phenomena*, edited by R. Hochstrasser, W. Kaiser, and C. V. Shank (Springer-Verlag, Berlin/II New York, 1980), Vol. 2, p. 249.
- ³³T. J. Chuang, G. W. Hoffman, and K. B. Eisenthal, *Chem. Phys. Lett.* **25**, 201 (1974).
- ³⁴R. Zadoyan, Z. Li, P. Ashjian, C. C. Martens, and V. A. Apkarian, *Chem. Phys. Lett.* **218**, 504 (1994).
- ³⁵R. Zadoyan, Z. Li, C. C. Martens, and V. A. Apkarian, *J. Chem. Phys.* **101**, 6648 (1994).
- ³⁶Q. Liu, J. K. Wang, and A. H. Zewail, *Nature* **364**, 427 (1993).
- ³⁷E. D. Potter, Q. Liu, and A. H. Zewail, *Chem. Phys. Lett.* **200**, 605 (1992).
- ³⁸D. J. Nesbitt and J. T. Hynes, *J. Chem. Phys.* **77**, 2130 (1982).
- ³⁹Q. L. Liu, J. K. Wang, and A. H. Zewail, *J. Phys. Chem.* **99**, 11321 (1995).
- ⁴⁰J. K. Wang, Q. L. Liu, and A. H. Zewail, *J. Phys. Chem.* **99**, 11309 (1995).
- ⁴¹D. A. V. Kliner, J. C. Alfano, and P. F. Barbara, *J. Chem. Phys.* **98**, 5375 (1993).
- ⁴²J. C. Alfano, Y. Kimura, P. K. Walhout, and P. F. Barbara, *Chem. Phys.* **175**, 147 (1993).
- ⁴³A. E. Johnson, N. E. Levinger, and P. F. Barbara, *J. Phys. Chem.* **96**, 7841 (1992).
- ⁴⁴M. A. Johnson and W. C. Lineberger, in *Techniques for the Study of Ion Molecule Reactions*, edited by J. M. Farrar and J. W. Saunders (Wiley, New York, 1988), pp. 591.
- ⁴⁵J. M. Papanikolas, V. Vorsa, M. E. Nadal, P. J. Campagnola, H. K. Buchenau, and W. C. Lineberger, *J. Chem. Phys.* **99**, 8733 (1993).
- ⁴⁶J. M. Papanikolas, V. Vorsa, M. E. Nadal, P. J. Campagnola, J. R. Gord, and W. C. Lineberger, *J. Chem. Phys.* **97**, 7002 (1992).
- ⁴⁷V. Vorsa, P. J. Campagnola, S. Nandi, M. Larsson, and W. C. Lineberger, *J. Chem. Phys.* **105**, 2298 (1996).
- ⁴⁸M. E. Nadal, P. D. Kleiber, and W. C. Lineberger, *J. Chem. Phys.* **105**, 504 (1996).
- ⁴⁹J. M. Papanikolas, P. J. Campagnola, V. Vorsa, M. E. Nadal, H. K. Buchenau, and W. C. Lineberger, in *Advances in Physical Chemistry, Vol. 6, The Chemical Dynamics and Kinetics of Small Radicals*, edited by K. Liu and A. Wagner (World Scientific, Singapore, 1995).
- ⁵⁰W. C. Lineberger, M. E. Nadal, P. J. Campagnola, V. Vorsa, P. D. Kleiber, J. M. Papanikolas, P. E. Maslen, J. Faeder, R. Parson, and O. Poplawski, in *Proceedings of The Robert A. Welch Foundation 38th Conference on Chemical Research: Chemical Dynamics of Transient Species*, Vol. 38 (R. A. Welch Foundation, Houston, Texas, 1994), pp. 175.
- ⁵¹J. M. Papanikolas, J. R. Gord, N. E. Levinger, D. Ray, V. Vorsa, and W. C. Lineberger, *J. Phys. Chem.* **95**, 8028 (1991).
- ⁵²D. Ray, N. E. Levinger, J. M. Papanikolas, and W. C. Lineberger, *J. Chem. Phys.* **91**, 6533 (1989).
- ⁵³M. L. Alexander, N. E. Levinger, M. A. Johnson, D. Ray, and W. C. Lineberger, *J. Chem. Phys.* **88**, 6200 (1988).
- ⁵⁴J. M. Papanikolas, P. E. Maslen, and R. Parson, *J. Chem. Phys.* **102**, 2452 (1995).
- ⁵⁵F. G. Amar and L. Perera, *Z. Phys. D* **20**, 173 (1991).
- ⁵⁶W. C. Wiley and I. H. McLaren, *Rev. Sci. Instrum.* **26**, 1150 (1955).
- ⁵⁷B. A. Mamyrin, V. I. Karataev, D. V. Shmikk, and V. A. Zagulin, *Sov. Phys.-JEPT* **37**, 45 (1973).
- ⁵⁸E. C. M. Chen and W. E. J. Wentworth, *J. Phys. Chem.* **89**, 4099 (1985).
- ⁵⁹J. G. Dojahn, E. C. M. Chen, and W. E. Wentworth, *J. Phys. Chem.* **100**, 9649 (1996).
- ⁶⁰M. R. Battaglia, A. D. Buckingham, D. Neumark, R. K. Pierens, and J. H. Williams, *Mol. Phys.* **43**, 1015 (1981).
- ⁶¹C. Kittel, *Introduction to Solid State Physics*, 6th ed. (Wiley, New York, 1986).
- ⁶²N. E. Levinger, D. Ray, M. L. Alexander, and W. C. Lineberger, *J. Chem. Phys.* **89**, 5654 (1988).
- ⁶³K. Hiraoka, *J. Chem. Phys.* **89**, 3190 (1988).
- ⁶⁴K. Hiraoka and T. Mori, *J. Chem. Phys.* **90**, 7143 (1989).